CMS Draft Analysis Note

The content of this note is intended for CMS internal use and distribution only

2008/10/08
Archive Id: 1.31
Archive Date: 2008/10/08 14:06:39

SUSY searches with dijet events

Henning Flächer[1], John Jones[2], Tanja Rommerskirchen[3], Benjamin Sinclair[1], and Markus Stoye[4]

[1] CERN, Geneva, Switzerland
[2] Princeton University, Princeton, USA
[3] University of Zürich, Zürich, Switzerland
[4] Imperial College, London, UK

Abstract

We present a search for supersymmetry (SUSY) in dijet events with the CMS detector at the LHC. Our study is focused on a SUSY parameter space where squarks are pair produced and both directly decay to a quark and neutralino with the latter escaping the detector, thus leaving a missing energy signature. Although the background from QCD dijet events is overwhelming the particular kinematics of the SUSY events allow the definition of powerful discriminating variables which could enable a discovery with the early physics data.

1 Introduction

In this note we present search strategies for a possible discovery of supersymmetric (SUSY) signatures at the LHC using dijet events. Apart from a number of other attractive features, SUSY presents an extension to the Standard Model which provides a stable neutral particle χ_1^0, a candidate for astrophysical cold dark matter which is in good agreement with the cosmological data. A new approach to SUSY searches with dijet events was recently proposed in Ref. [1]. It is based on the assumption that squarks are pair produced and subsequently decay directly to a quark and the χ_1^0, the lightest stable particle (LSP). This approach is most promising for points in a SUSY parameter space where squarks have large branching fractions to decay directly to the LSP. This in turn requires the gluino to be heavier than the squarks, thus avoiding cascade decays of squarks via the gluino.

The event topology under investigation consists of two high-p_{T} jets and two invisible neutralinos which lead to a missing energy signature. The main background processes for this topology are QCD dijet events and Z + jet events where the Z decays into two neutrinos. As we will show it is however possible to define kinematic variables that can discriminate between signal and background without relying on the missing energy measurement from the calorimeters. The analysis presented here is an extension to the existing SUSY searches within CMS which so far have focused on missing E_{T} signatures with ≥ 3 jets and/or involving charged leptons [2]. With sufficient integrated luminosity it will be possible to constrain the squark and neutralino masses from dijet events (see Ref. [1] for more details), this however is beyond the scope of this note.

This note is organized as follows: In Section 2 we describe the analysis framework and the Monte Carlo (MC) data samples used to produce the results presented here. In Section 4 the event selection is described followed by a description of the analysis method and the results in Section 5. Furthermore we discuss the data-driven methods that were developed for background estimation in Section 7 and give the results of our systematic studies in Section 6 before concluding.

2 Analysis Framework

The code used in this analysis was developed on top of the SusyAnalysis framework [3], which is itself an extension of the Physics Analysis Toolkit (PAT) [4]. The PAT provides post-processing on reconstructed event data to clean it and condense the number of objects in an event, thereby simplifying user analysis. The framework comprises three layers: the initial layer reprocesses RECO or AOD data, for example removing duplicate objects from collections. It also associates the reconstructed objects to Monte Carlo truth information and trigger objects.

The second layer condenses the cleaned and associated data into simple object collections, such as PAT::Jet, PAT::Electron and PAT::Muon, sorted by uncorrected transverse energy. At this stage the data is available for use in analysis.

The third layer is optionally used and can be combined with custom steps in a user's analysis code. It includes a cross-cleaning module to eliminate overlaps between objects sharing common energy deposits such as jets and electrons, and to correct their energies appropriately. The cross-cleaner operates by generating an association map between different types of PAT object along with criteria for either the removal of an object from the collection or the modification of its energy depending on a corresponding change in another object.

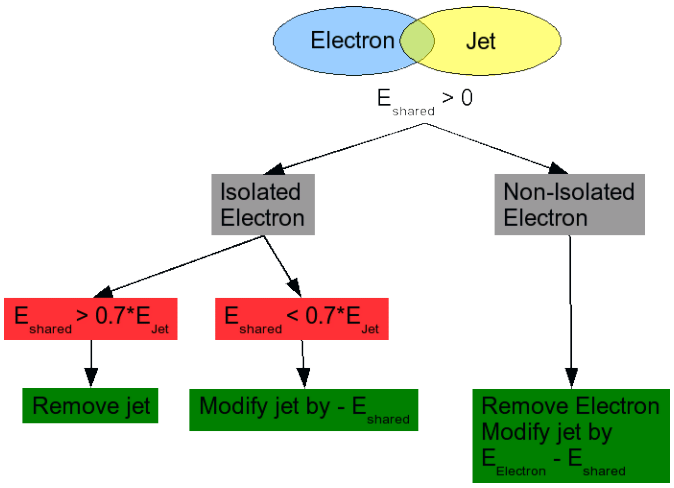

Figure 1: An example of cross-cleaning, showing the electron-photon case.

As an example, consider the jet-electron case (as shown in Figure 1). Firstly, one finds the jet nearest to an electron in the calorimeter. If they share at least one energy deposit, they are associated. For an isolated electron, if more than 70% of the electron's energy is shared with the jet, the jet object is removed. If less than 70%, the jet's energy is reduced by an amount equal to the shared energy. For a non-isolated electron, the electron is removed and any additional energy shared by the electron is added to the jet. The full list of cases handled by the cross-cleaner are:

- Electron-jet.
- Photon-jet.
- Muon-jet.
- Electron-jet.
- Electron-photon.

In addition to this, whenever the jet collection is changed, the MET calculation is modified accordingly. Further information on the cross-cleaning module can be found on the CMS twiki [5]. In the analysis presented here we make use of the electron-jet and muon-jet cross-cleaning modules.

Once these stages are completed, the cleaned and corrected objects are used by the SusyAnalysis framework to generate a ROOT file containing variables of interest for analysis based on different cuts, and a set of stored counts of whether an event passed a cut or failed it, as well as an overall decision over whether the data is selected.

Analysis variables are encapsulated by EventSelector classes which, given the necessary PAT data, provide a boolean result indicating whether the variable passes a cut, as well as providing the calculated variable itself for storage in the output file. It is then a relatively simple task to decimate the event data sufficiently to permit local storage of the results for further analysis. Many selectors are provided for general use in analysis in addition to those used in event selection in this analysis. This analysis uses the AlphaSelector, DPhiSelector, JetEventSelector, MaxNumJetsEventSelector and LeptonVetoSelector.

3 Monte Carlo Data Samples

The data for this analysis has been taken from the CSA07 data challenge [6]. Several data sets have been used in this analysis. The background data can be divided into three main data sets. Two of these are the 'gumbo' and 'chowder' soups, the third is the background contribution from $Z \rightarrow \nu\bar{\nu}$ events.

- Gumbo contains the basic QCD processes generated using Pythia [7], split into minimum bias and high-energy jet data.
- Chowder includes $t\bar{t}$+jet, W+jet, and Z+jet channels simulated using ALPGEN [8] to more accurately model higher-order QCD corrections. In addition to the events included in the soups, we include additional W+jet and Z+jet MC samples produced in bins of the W/Z p_T between $300 - 3200\,\text{GeV}$ for jet multiplicities ranging from $1 - 5$ [9].
- The third data set is a Pythia-generated $Z \rightarrow \nu\bar{\nu}$ sample, generated in 21 bins of $\hat{p_T}$ ranging from $0 - 15\,\text{GeV}$ to $> 3500\,\text{GeV}$ [9]. This process represents an important irreducible background in this analysis, as discussed later in this note.

In addition, single top, γ + jets and $b\bar{b}$ + jets background samples were investigated. It was found, however, that they only play a negligible role in the presented search.

The low mass mSuGra SUSY test points are used to estimate signal significance for various points in the SUSY parameter space. A summary of these parameters is shown in Table 1.

Table 1: Definition of low mass SUSY points. Cross sections were estimated using PROSPINO1 [10]. The last two columns give the masses of the lightest squark and the lightest neutralino, χ_1^0.

Sample	m_0 (GeV)	$m_{1/2}$ (GeV)	A_0	$\tan\beta$	sign(μ)	σ NLO (pb)	(LO) (pb)	lightest $\tilde{q}$ (GeV)	χ_1^0 (GeV)
LM1	60	250	0	10	+	54.86	(43.28)	410 ($\tilde{t}_1$)	97
LM2	185	350	0	35	+	9.41	(7.27)	582 ($\tilde{t}_1$)	141
LM3	330	240	0	20	+	45.47	(34.20)	446 ($\tilde{t}_1$)	94
LM4	210	285	0	10	+	25.11	(19.43)	483 ($\tilde{t}_1$)	112
LM5	230	360	0	10	+	7.75	(5.96)	603 ($\tilde{t}_1$)	145
LM6	85	400	0	10	+	4.94	(3.84)	649 ($\tilde{t}_1$)	162
LM7	3000	230	0	10	+	6.79	(3.82)		
LM8	500	300	-300	10	+	12.19	(8.81)	546 ($\tilde{t}_1$)	121
LM9	1450	175	0	50	+	39.79	(23.28)		

To summarise, the datasets used are:

- QCD (Pythia).
- $t\bar{t}$+jet,W+jet,Z+jet including W,Z samples with $p_T > 300\,\text{GeV}$ (ALPGEN).
- $Z \rightarrow \nu\bar{\nu}$ (Pythia).
- SUSY LM1-9 (Pythia).

4 Event selection

We use the cross-cleaned collections described in the previous section to define our physics objects, in particular jets and leptons described below. In addition we use two HLT trigger paths to select our events of interest.

- Trigger:
  Two trigger paths are used for event selection in this analysis. The first of these is the HLT1jet path. The L1 trigger criterion for the HLT1jet path is a L1_SingleJet150 condition (i.e. a single jet with an E_T greater than 150 GeV). At the HLT level this cut is raised to 200 GeV, reflecting the increasing sophistication of the jet finding algorithm. There is no cut on other jets in this path - this is achieved during preselection in this analysis. For the HLT2jet path, the L1 conditions are either Ll_SingleJet150 or L1_DoubletJet70 (i.e. two jets with E_T greater than 70 GeV). At the HLT level this cut is raised to two jets with E_T greater than 150 GeV, significantly higher than the preselection cuts in this analysis, but a necessary consequence of the current trigger paths.
- Jet definitions:
  As jet collection we use corrected iterative cone $R = 0.5$ jets (iterativeCone5CaloJets) where we require two jets with $p_{\mathrm{T}} > 50$ GeV and an electromagnetic fraction F_{em} less than 0.9.
- Missing momentum based on jets:
  Based on the two leading jets we define two additional variables: HT as the scalar sum of the two leading jet p_{T}'s, HT = $p_T^{j1} + p_T^{j2}$ and calculate a missing p_{T} (MHT) of the event as $\vec{\mathrm{MHT}} = -(\vec{p_T^{j1}} + \vec{p_T^{j2}})$.
- Lepton veto:
  We veto any event where either an electron, muon or tau with momentum $p_{\mathrm{T}} >$ 10 GeV was identified. The default PAT options [5] are used for the lepton reconstruction.

In order to select "clean" dijet events we veto against events with any additional jets with $p_{\mathrm{T}} > 50$ GeV. To protect against significant mis-measurements of jet energies we veto events where the missing p_{T} based on the two jet system points into the same direction as one of the first three jets, $\Delta\phi(\mathrm{j}, \mathrm{MHT}) < 0.3$ rad. Our definition of missing E_{T} based on the two jet momenta should also be robust against fake signals and noise in the calorimeters. In addition to the selection criteria above we require the leading jet to be within $|\eta| < 2.5$.

To summarise, this results in the following preselection:

- $p_T^{j1} > 50$ GeV, $p_T^{j2} > 50$ GeV
- $F_{\mathrm{em}}^{j1} < 0.9$, $F_{\mathrm{em}}^{j2} < 0.9$
- $|\eta_{\mathrm{j1}}| < 2.5$
- $p_T^{j3} < 50$ GeV
- $\Delta\phi(\mathrm{j_i}, \mathrm{MHT}) < 0.3$ rad (i=1,2,3)
- $p_{\mathrm{T}}^{e} < 10$ GeV, $p_{\mathrm{T}}^{\mu} < 10$ GeV, $p_{\mathrm{T}}^{\tau} < 10$ GeV

The p_{T} and η distributions of the two leading jets after preselection are shown in Figure 2.

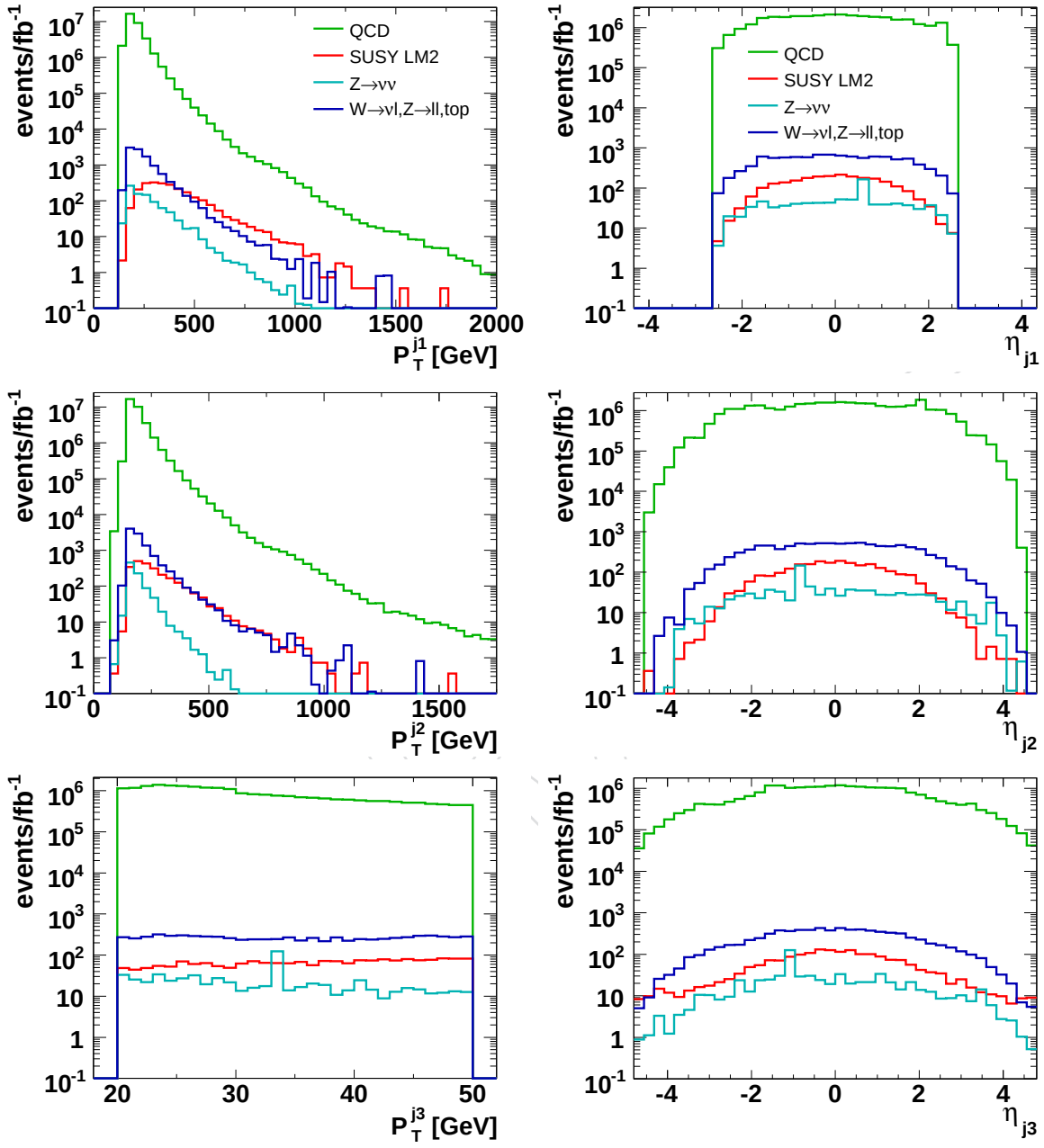

Figure 2: Distribution of p_{T} and η for the two leading jets and a possible third jet after preselection.

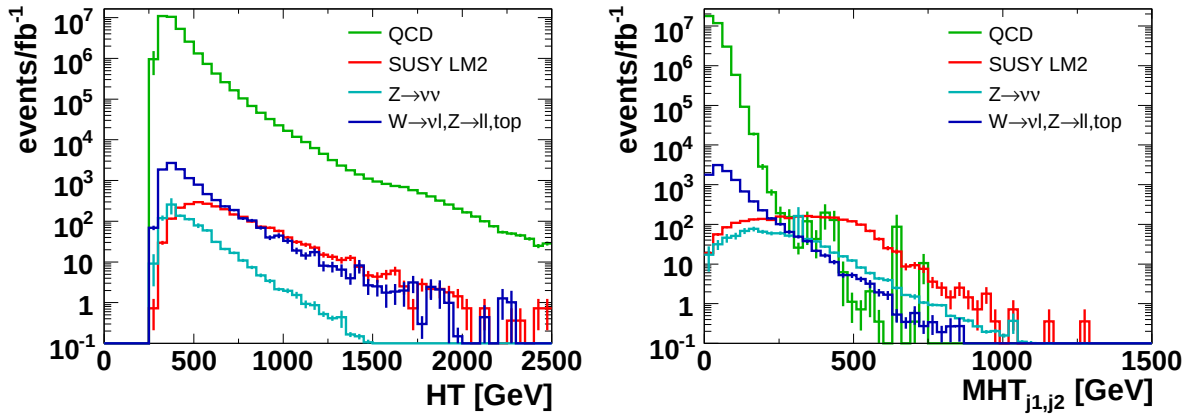

Figure 3: Distribution of HT after preselection (left) and MHT after requiring HT $>$ 500 GeV (right).

5 Analysis Method and results

5.1 Event kinematics

As mentioned in the previous section the HLT2jet trigger requires already two (uncorrected) jets with $p_T > 150$ GeV each, which implies HT $\gtrsim 300$ GeV. While we give in this Section expected event yields for both, the HLT2jet trigger and the combination of HLT2jet and HLT1jet, all the figures are made requiring the HLT2jet trigger to be passed which we define as our default scenario. For signal events we expect two high-p_T jets coming directly from a squark decay with typical masses > 600 GeV. Therefore, to further reduce background contributions we require HT > 500 GeV. The HT distribution is shown in Figure 3 together with the MHT distribution after the cut on HT.

Even after requiring two high-p_T jets, there are sizable background contributions from a number of processes, the most important of which are:

- QCD dijet events due to their (overwhelmingly) large cross-section and sizable uncertainties in higher-oder corrections, in particular production of extra jets due to gluon emission.
- $Z \rightarrow \nu\bar{\nu}$ events which present an irreducible background as the invisible Z decay leads to real missing E_T.
- In addition, W+jet events contribute, when the W decays leptonically and the charged lepton was either not reconstructed or outside the detector acceptance.

It is however possible to define kinematic variables which separate between QCD events and signal-like events with real missing E_T. In well measured QCD dijet events, transverse momentum conservation requires the p_T of the two jets to be of equal magnitude and back-to-back in ϕ. These requirements do not apply to signal-like events where, the two squarks decay independently and therefore the resulting jet p_T's can be of different magnitude and also their ϕ values are (largely) uncorrelated. The difference in the azimuthal angle ϕ for the background processes and the low mass SUSY point LM1, defined in Table 1 is shown in Figure 4.

In Ref. [1] a new variable α was suggested which exploits the requirement of back-to-back jets of equal magnitude for QCD events:

$$\alpha = E_T^{j2} / M_{\text{inv}}^{j1,j2} \tag{1}$$

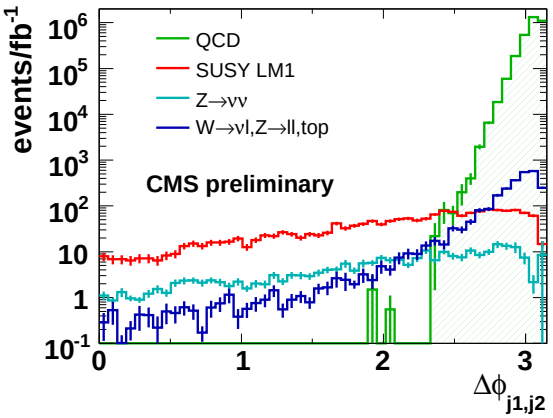

Figure 4: Distribution of $\Delta\phi_{j1,j2}$, after application of all selection cuts apart from the one on α (α_T).

For massless particles this is equal to

$$\alpha = \frac{E_T^{j2}}{\sqrt{2E^{j1}E^{j2}(1-\cos\Phi)}}, \tag{2}$$

where Φ is the angle between the two jets. As can be seen from Eq. 2, α can at most have a value of 0.5 for well measured QCD events. In addition, as the E_T of the second energetic jet enters in the numerator uncertainties introduced through energy mismeasurements partly cancel out in α (if one of the two jet energies is measured wrong by a large amount the order of the two jets will be swapped). In our analysis we also explore a modified version of this variable where we use the transverse mass of the two jets instead of the invariant mass:

$$\alpha_T = E_T^{j2} / M_{\text{inv}}^{j1,j2}{}_T \tag{3}$$

Again, for massless particles this can be rewritten as

$$\alpha_T = \frac{E_T^{j2}}{\sqrt{2E_T^{j1}E_T^{j2}(1-\cos\Delta\phi)}} = \frac{\sqrt{E_T^{j2}/E_T^{j1}}}{\sqrt{2(1-\cos\Delta\phi)}} \tag{4}$$

where $\Delta\phi$ is the difference in azimuthal angle of the two jets. For well measured QCD dijet events α_T is exactly 0.5. The α and α_T distributions are shown in Figure 6 for the different background processes and exemplary for LM1. The two-dimensional distribution of E_T^{j2}/E_T^{j1} vs $\Delta\phi$ which enter into α_T (cfg. Eq. 4) is shown in Figure 5 for the different background processes and exemplary for the low mass SUSY point LM1. While from Figures 4 and 5 one might get the impression that it would be sufficient to require $\Delta\phi \lesssim 2\pi/3$ rad we prefer to use α and α_T instead. In particular in the case of QCD dijet events additional hard and soft gluon emission is associated with significant uncertainties which alters the $\Delta\phi$ distribution for such events. A detailed study by the DØ experiment [11] found sizable differences in the modeling of these higher order effects by Monte Carlo event generators when compared with the data. While our selection is safe with respect to the effects of hard extra gluon radiation by rejecting events with extra jets with $p_T > 50$ GeV, multiple soft gluon emission might still lead to large enough effect to alter the $\Delta\phi$ distribution. Compared with $\Delta\phi$, α and α_T have the additional benefit that they are more effective in rejecting $Z \to \nu\bar{\nu}$events. In the following we will therefore use α and α_T,

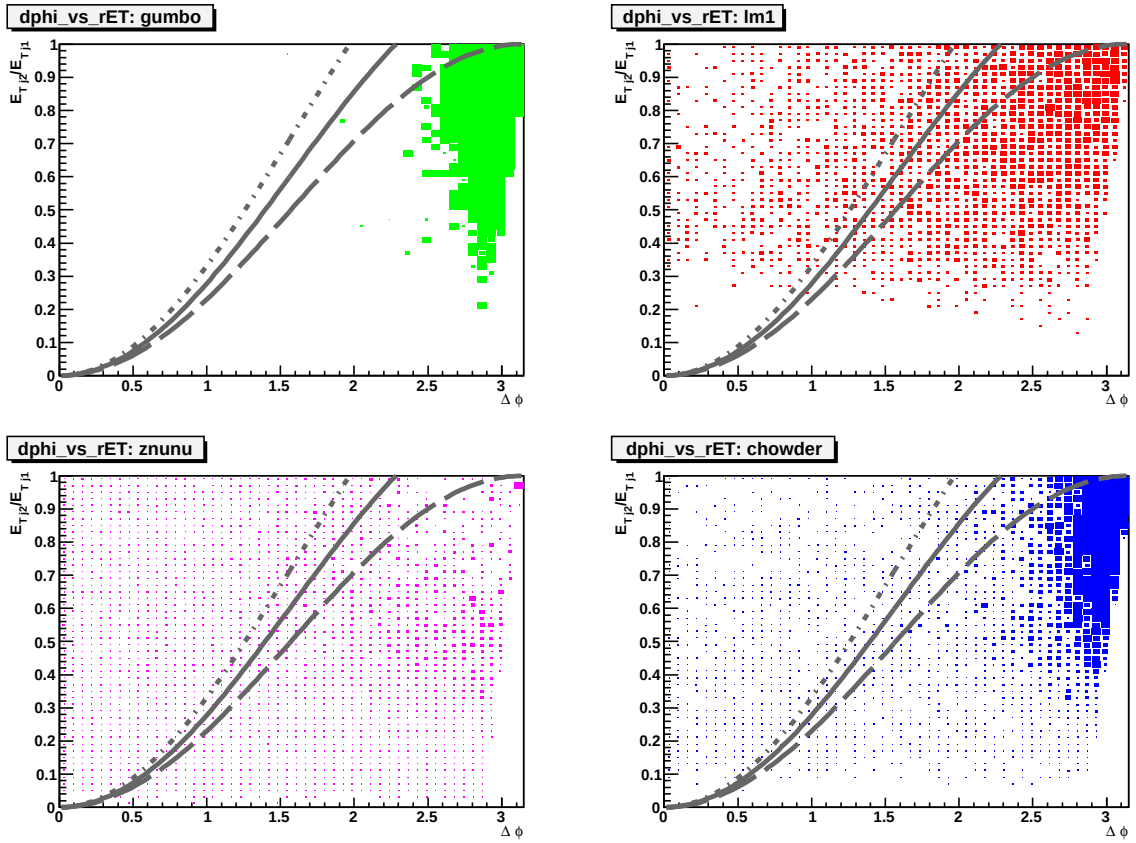

Figure 5: Ratio of the two leading jet E_T's versus $\Delta\phi_{j1,j2}$ for the different backgrounds and LM1 signal sample. Upper left: QCD, upper right: LM1, lower left: $Z \rightarrow \nu\bar{\nu}$, lower right: $t\bar{t}$,W,Z events. The solid line indicates a value of $\alpha_T = 0.55$, while the dashed line corresponds to values of $\alpha_T = 0.5$ and the dotted line to $\alpha_T = 0.6$.

shown in Figure 6 in our event selection which in addition also reject events where the p_T of the two jets is not balanced. Both variables are highly correlated to $\Delta\phi$, so an additional cut on $\Delta\phi$ has only a negligible effect.

To account for finite jet energy and ϕ resolution we require $\alpha\,(\alpha_T) > 0.55$. For the full event selection we therefore require the following cuts on top of the preselection:

- HT $> 500\,\text{GeV}$
- $\alpha > 0.55$ or $\alpha_T > 0.55$ and $\Delta\phi_{j1,j2} < 2\pi/3$

5.2 Expected background from Monte Carlo simulations

Applying the selection criteria described above we obtain the events numbers listed in Table 2 at different stages of the event selection. All the numbers correspond to a data sample of $1\,\text{fb}^{-1}$.

It can be seen that both α and α_T are very effective in reducing the backgrounds, particularly from QCD dijet events but also for electroweak processes. When using α_T instead of α the signal yield for the LM1 point is almost doubled, however the dominant background from $Z \rightarrow \nu\bar{\nu}$ rises by about a factor 3 while the background from $t\bar{t}$, W, and Z decays doubles as well. We therefore propose to study both variables with real data as the signal to background ratio differs in the two cases. Nevertheless, in each case we observe signal over background

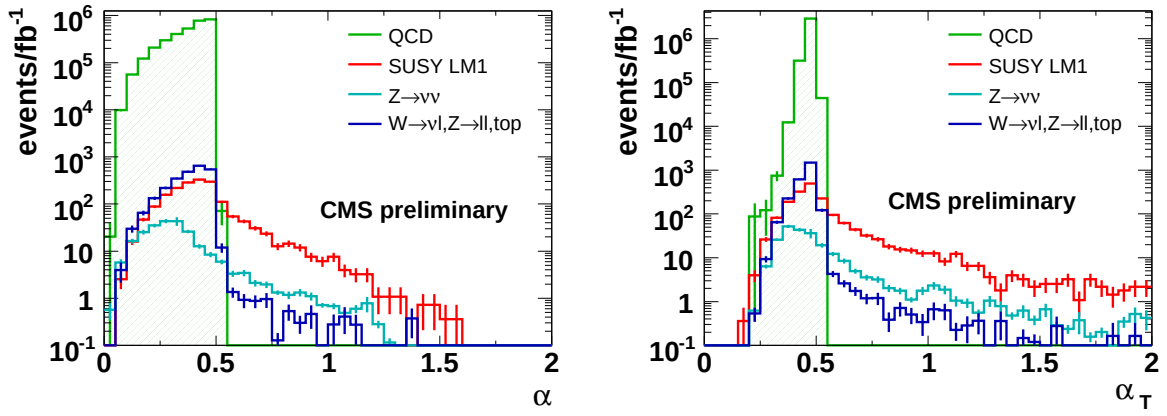

Figure 6: Distribution of α and α_T after all other selection cuts have been applied.

Table 2: Expected number of events after each selection cut for background samples (QCD, $t\bar{t}$,W,Z+jets, and $Z \rightarrow \nu\bar{\nu}$) and LM1 signal point. The final numbers of selected events are shown after a cut on α or alternatively α_T and $\Delta\phi_{j1,j2}$.

	HLT2jet				HLT2jet || HLT1jet			
Selection cut	QCD	$t\bar{t}$,W,Z	$Z \rightarrow \nu\bar{\nu}$	LM1	QCD	$t\bar{t}$,W,Z	$Z \rightarrow \nu\bar{\nu}$	LM1
Trigger	1.1×10^8	147892	1807	25772	1.4×10^8	225351	8207	34757
Preselection	3.4×10^7	9820	878	2408	3.5×10^7	16002	4469	3583
HT > 500 GeV	3.2×10^6	2404	243	1784	3.2×10^6	2562	421	2099
$\alpha > 0.55$	0	7.2	19.7	227.6	0	10.1	26.1	248.8
$\alpha_T > 0.55$	0	19.9	58.2	439.6	0	29.3	83.7	527.9
$\Delta\phi_{j1,j2} < 2\pi/3$	0	18.7	57.2	432.4	0	28.1	82.6	520.7

ratios > 5.

5.2.1 Comment on GEANT simulation bug

While carrying out our studies on the CSA07 MC samples we learned of an implementation problem of the GEANT package in CMSSW that affects all MC samples. The problem affects long lived particles that travel further than 10 cm before decaying, mostly b- and c- hadrons and some τs. The decay products of these particles are saved in the wrong reference frame (that of the mother instead of the laboratory frame) which leads to jets from high-p_T particles of $p_T > 100$ GeV to be reconstructed as very low p_T particles of a few GeV. For a detailed discussion of this problem see [12]. In the course of our analysis we found a small number of QCD events where $\Delta\phi_{j1,j2}$ was much smaller than π and the difference in the two jet E_T was quite large. For each of these events we then noticed that the missing HT vector was pointing in the direction of a low p_T jet. In addition, we noticed that each of these low p_T jets can be ΔR matched to a true b-jet with $p_T > 100$ GeV. We therefore exclude events with a true b hadron with $p_T > 100$ GeV and matched to a reconstructed jet within $\Delta R < 0.5$ if the reconstructed p_T is less than 20% of the true p_T.

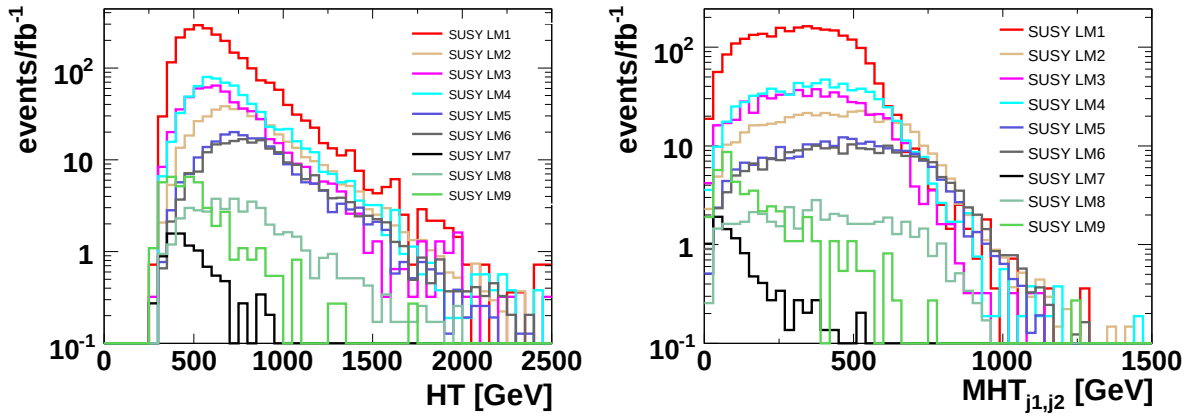

Figure 7: Distribution of HT after preselection (left) and MHT after an requiring HT $>$ 500 GeV for the different low mass SUSY points (right).

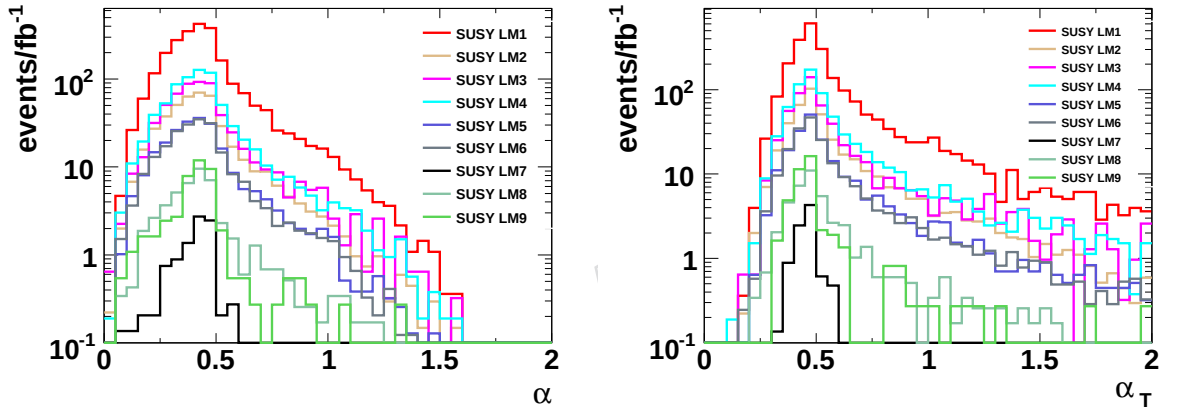

Figure 8: Distribution of α and α_T for the different low mass SUSY points after all other selection cuts have been applied.

5.3 Event yields for low mass SUSY signal samples

In addition to the mSuGra point LM1 we also studied expected event yields for the other low mass SUSY points LM2-LM9 which are summarised in Table 3 where the selection on α_T was used and the HLT2jet trigger required. Figures 7 and 8 show the HT, MHT, and α and α_T distributions for the studied LM points, respectively.

From Table 3 it can be seen that also for LM4 a signal over background ratio $>$ 2 can be achieved while for LM2 and LM3 the signal would still dominate over the expected background. In addition to the expected event yields we studied the underlying production process and subsequent decay for events surviving our selection criteria to verify that our selection procedure is mainly sensitive to the decay $\tilde{q} \to q\chi_1^0$. We define the following 6 categories:

- $\tilde{q}\,\tilde{q}$ (invisible):
  production process is $\tilde{q}\,\tilde{q}$ and both squarks decay to quark + invisible, either directly via $\tilde{q} \to \chi_1^0 q$ or $\tilde{q} \to \chi_2^0 q$ followed by $\chi_2^0 \to \chi_1^0 \nu\bar{\nu}$
- $\tilde{q}\,\tilde{q}$ (other):
  production process is $\tilde{q}\,\tilde{q}$ where at least one of the squarks decays to a quark + visible

Table 3: Expected event yields for specific low mass SUSY points after selection on α_T and the HLT2jet trigger, normalised to $1\,\text{fb}^{-1}$. In addition the relative contribution from the different production processes to the selected signal is shown.

Sample	Events	$\tilde{q}\,\tilde{q}$ (invisible)	$\tilde{q}\,\tilde{q}$ (other)	$\tilde{q}\,\tilde{g}$ (invisible)	$\tilde{q}\,\tilde{g}$ (other)	$\tilde{g}\,\tilde{g}$	other
LM1	432	39%	22%	18%	16%	3%	1%
LM2	132	46%	33%	9%	9%	0%	2%
LM3	138	69%	17%	4%	8%	0%	2%
LM4	195	49%	10%	29%	7%	3%	1%
LM5	76	69%	10%	16%	3%	1%	1%
LM6	68	66%	18%	8%	2%	0%	6%
LM7	0.4	0%	0%	0%	0%	0%	100%
LM8	13	56%	32%	0%	9%	0%	3%
LM9	5	0%	0%	0%	0%	0%	100%

Table 4: Relative contribution of different production processes for the LM1 point when varying the requirement on the third jet p_T.

Production process	$p_T^{j3} < 30\,\text{GeV}$	$p_T^{j3} < 50\,\text{GeV}$	$p_T^{j3} < 70\,\text{GeV}$
$\tilde{q}\,\tilde{q}$	80%	61%	51%
$\tilde{q}\,\tilde{g}$	18%	34%	44%
$\tilde{g}\,\tilde{g}$	1%	3%	5%

particles

- $\tilde{q}\,\tilde{g}$ (invisible):
  production process is $\tilde{q}\,\tilde{g}$, with $\tilde{g} \to \tilde{q}q$, followed by $\tilde{q} \to q$ + invisible particles for both squarks as in the first category
- $\tilde{q}\,\tilde{g}$ (other):
  production process is $\tilde{q}\,\tilde{g}$ with at least one of the resulting squarks decaying to quark + visible particles
- $\tilde{g}\,\tilde{g}$:
  production process is $\tilde{g}\,\tilde{g}$
- other :
  all other production processes

The results are summarised in Table 3. It can be seen that for most of the models studied, the pair production of squarks and their subsequent decay to a quark + invisible particles is the dominant contribution as would be expected. For both LM7 and LM9 the $\tilde{q}$'s are very heavy (and much heavier than the $\tilde{g}$) and hence a direct decay to a quark + LSP is not expected. The relatively large contributions from $\tilde{q}\,\tilde{q}$ (other) can be attributed to χ_1^+ decays to χ_1^0 in which, due to the small mass differences, a low p_T charged lepton is produced that remains undetected.

The contribution from $\tilde{q}\,\tilde{g}$ production can be attributed to $\tilde{g} \to \tilde{q}q$ decays where the additional jet from the $\tilde{g}$ decay is relatively soft because of the small mass difference between $\tilde{q}$ and $\tilde{g}$. To test this assumption we have varied the requirement on the p_T of the third jet, changing it by $\pm 20\,\text{GeV}$. The results are shown in Table 4. As expected the contribution from $\tilde{q}\,\tilde{q}$ is enhanced when lowering the third jet veto to 30 GeV while it is reduced when increased to 70 GeV.

6 Systematic studies

6.1 Jet-Energy scale and resolution

To estimate the systematic uncertainties due to miscalibration additional jet measurement uncertainties and biases have been studied:

- a Gaussian smearing of the transverse momenta of 10% and a Gaussian smearing of the azimuthal angle ϕ by 0.1 rad.
- a scaling of the jet energy scale by $\pm$ 5%.
- a scaling of the jet energy scale in the forward direction ($|\eta > 1.4|$) by $\pm$ 3%.

The results are summarized in Table 5. The Gaussian smearing effects the efficiency, but the signal to noise ratio remains similar. The upward scaling of the transverse momenta of the jets effectively relaxes the HT cut and hence more events pass the selection. The reduced momentum leads hence to less events. The miscalibration applied for the jet energy scale in the forward regions has a negligible effect. Overall the signal to background ratio remains stable under varying conditions and the background from QCD remains small in all scenarios.

Table 5: Event yields after jet-miscalibration procedures

	LM1	$Z \rightarrow \nu\bar{\nu}$	$t\bar{t}$,W+jets,Z+jets	QCD	S/B
default	432	57	19	0	5.6
10% smeared	421	55	18	0	5.4
+ 5% scaled	455	67	23	0	5.0
- 5% scaled	378	49	15	0	5.9
forward +3% scaled	432	58	18	0	5.6
forward -3% scaled	432	55	18	0	5.8

6.2 Higher order QCD effects: Comparison of matrix element calculation with PYTHIA parton shower

In order to reliably extract event yields for the presented dijet analysis a good understanding of the emission of extra (hard) jets is necessary. If the rate of extra jets with momentum $p_T >$ 50 GeV is larger than what is assumed in our simulations these events will get rejected by the third jet veto. This is of particular importance for signal events.

For the MC samples used in this analysis the emission of extra jets is taken care of by PYTHIA which uses a phenomenological parton-shower model to simulate higher order QCD effects. A more sophisticated approach is to use a matrix-element calculation where the emission of extra ISR gluons is already done within the matrix-element which then need to be matched to a jet. A study comparing the two approaches was carried out by Simon de Visscher (Universite catholique de Louvain) for the LM1 SUSY point in order to obtain an estimate of the systematic uncertainty related to higher order QCD effects.

The "matched" productions are done using MadGraph/MadEvent 4.3 to generate the squarks pairs and squark-gluino pairs with up to two additional ISR's at parton level. These events are then passed through PYTHIA to execute the matching procedure, i.e. reject events for which there is an overlap between the phase-spaces occupied by the parton shower simulation and the matrix element calculation.

For the "parton shower only" production we use Madgraph to generate the kinematics of the

two SUSY particles and let PYTHIA do the showering and notably the ISR generation. This results in two sets of samples for each process ($\tilde{q}\,\tilde{q}$, $\tilde{q}\bar{\tilde{q}}$ and $\tilde{q}\,\tilde{g}$), one with matching and one without. For each sample the hadrons are then clustered into jets directly at pythia output level, using a cone algorithm with the same parameters as in the CSA07 MC samples ($R = 0.5$, $p_{\mathrm{T}\,\mathrm{min}} = 15\,\mathrm{GeV}$).

These samples are then passed through an event selection resembling the preselection described in Section 4:

- 2 jets with $p_{\mathrm{T}} > 50\,\mathrm{GeV}$
- $p_T^{j3} < 50\,\mathrm{GeV}$
- $p_{\mathrm{T}}^{e} < 10\,\mathrm{GeV}$, $p_{\mathrm{T}}^{\mu} < 10\,\mathrm{GeV}$, $p_{\mathrm{T}}^{\tau} < 10\,\mathrm{GeV}$
- $|\eta_{jets,lept}| < 3$

As a result we find that the matched results give harder jets. Quantitatively, this results in a reduction of the selection efficiency by $\sim 12\%$ and $\sim 18\%$ for the $\tilde{q}\,\tilde{q}$ and $\tilde{q}\bar{\tilde{q}}$ production process, respectively, when the 2 hardest ISRs are simulated with the matrix-element calculation. Similarly, for the $\tilde{q}\,\tilde{g}$ production we find a reduction in efficiency of $\sim 7\%$. Of course the above excercise is only a coarse estimate but assuming a reduced signal efficiency due to higher order QCD effect of about $10 - 15\%$ seems reasonable. This however means that in case a low mass SUSY signal is present in the data it could be observed with dijet events.

7 Data-driven background estimation

In the following we describe the data-driven methods for background estimation in this analysis. The main emphasis is on an approach where signal enhanced and depleted regions in phase space are defined and the combination of all backgrounds can be estimated simultaneously. In a second approach that can serve as a cross-check, we describe how $\mathrm{W} \to \mu\nu$ events can be used to determine the size of the dominant $\mathrm{Z} \to \nu\bar{\nu}$ background. The background estimations described here are carried out for an event selection using α_{T} and the HLT2jet trigger.

7.1 Background estimation using the η dependence of α_{T} via the matrix method

The idea of the matrix method is to find two variables, $\mathcal{V}_1$ and $\mathcal{V}_2$, which are uncorrelated for background events and for which in the 2-d plane three quadrants exists that are signal depleted and one that is signal enriched, i.e. each variable has a signal enriched and a signal depleted region. In this case it is possible to determine the amount of background events directly from the data.

Let us consider events in the background depleted region of $\mathcal{V}_1$. We can split these events into those with values corresponding to the signal enriched region of $\mathcal{V}_2$ (A) and those with values in the signal depleted region of $\mathcal{V}_2$ (B). As $\mathcal{V}_1$ and $\mathcal{V}_2$ are assumed to be uncorrelated for background, the ratio A/B is constant for any value of $\mathcal{V}_1$. Therefore A/B is equal to C/D, the ratio of signal enriched (C) over signal depleted (D) background events of $\mathcal{V}_2$, now in the signal enriched region of $\mathcal{V}_1$. That is, the number of background events in the signal enriched region of both variables (C) can be determined as $C = A/B \times D$.

The two variables in question for our analysis are the the pseudo-rapidity η of the leading jet and α_{T}. As can be seen from Figure 9 the leading jet from a SUSY event is on average more central than those from the background processes, QCD, $\mathrm{t\bar{t}}$, W, Z+jets and $\mathrm{Z} \to \nu\bar{\nu}$. Therefore, the forward regions with $|\eta| > 2.5$ are considered as signal depleted. Similarly, we define

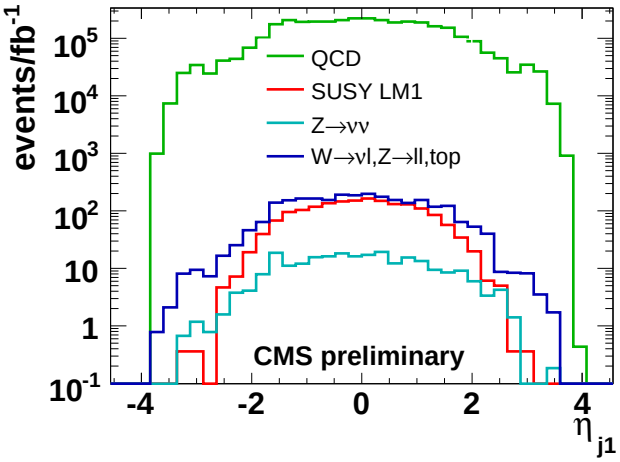

Figure 9: Distribution of η for QCD, $t\bar{t}$, W, Z, and SUSY events. Shown is the expected number of events for a luminosity of 1fb^{-1}, after all selection cuts except the cut on α_T

$\alpha_T > 0.55$ as signal enriched and $\alpha_T < 0.55$ as signal depleted regions. The α_T distribution in bins of $|\eta|$ is shown in Figure 10 where it can be seen that the shape of α_T does not change with $|\eta|$ as required for uncorrelated variables.

We define $R^i_{\alpha_T}$ as the ratio of events with $\alpha_T > 0.55/\alpha_T < 0.55$ for a given region bin i in $|\eta|$ which should be constant for the method outlined above to be applicable.

In real data it will not be possible to distinguish the different background processes on an event-by-event basis. It is therefore necessary to convince ourselves that the procedure outlined above is applicable to all the relevant background components if we are to determine the sum of all backgrounds with the help of the matrix method.

7.1.1 α_T versus $|\eta|$ for different background processes

For the matrix method to work α_T and η need to be uncorrelated for all backgrounds.

- QCD events:
  Figure 11 shows α_T versus $|\eta|$ of the leading jet for QCD events after all selection cuts except the cut on α_T and $|\eta|$ of the leading jet have been applied. No dijet events with $\alpha_T > 0.55$ remain. Therefore, in order to study the correlation between $\alpha_T > 0.55$ and $|\eta|$ of the first jet we relax the cut on $p_T^{j3}$to $< 200\,\text{GeV}$ to increase the statistics. Figure 11 also shows R_{α_T} as a function of $|\eta|$ and is observed to be approximately constant. This confirms that the two variables α_T and $|\eta|$ are uncorrelated.
- $t\bar{t}$, $W \to \ell\nu$ and $Z \to \ell\ell$ events:
  Figure 12 shows α_T versus $|\eta|$ for $t\bar{t}$, $W \to l\nu$ and $Z \to ll$ events after the application of all selection cuts except the cut on α_T and $|\eta|$ of the leading jet. Due to neutrinos which escape the detector, α_T is greater than 0.55 for some events with 2jets. Figure 12 also shows R_{α_T} as a function of $|\eta|$ after all selection cuts except the cut on α_T and $|\eta|$. The ratio stays to a good approximation constant with $|\eta|$
- $Z \to \nu\bar{\nu}$ Events:
  Figure 13 shows α_T versus $|\eta|$ for $Z \to \nu\nu$ events after the application of all selection cuts except the cuts on α_T and $|\eta|$ of the leading jet . Due to the two neutrinos in the events no sharp edge at $\alpha_T = 0.5$ is visible and the events are relatively evenly

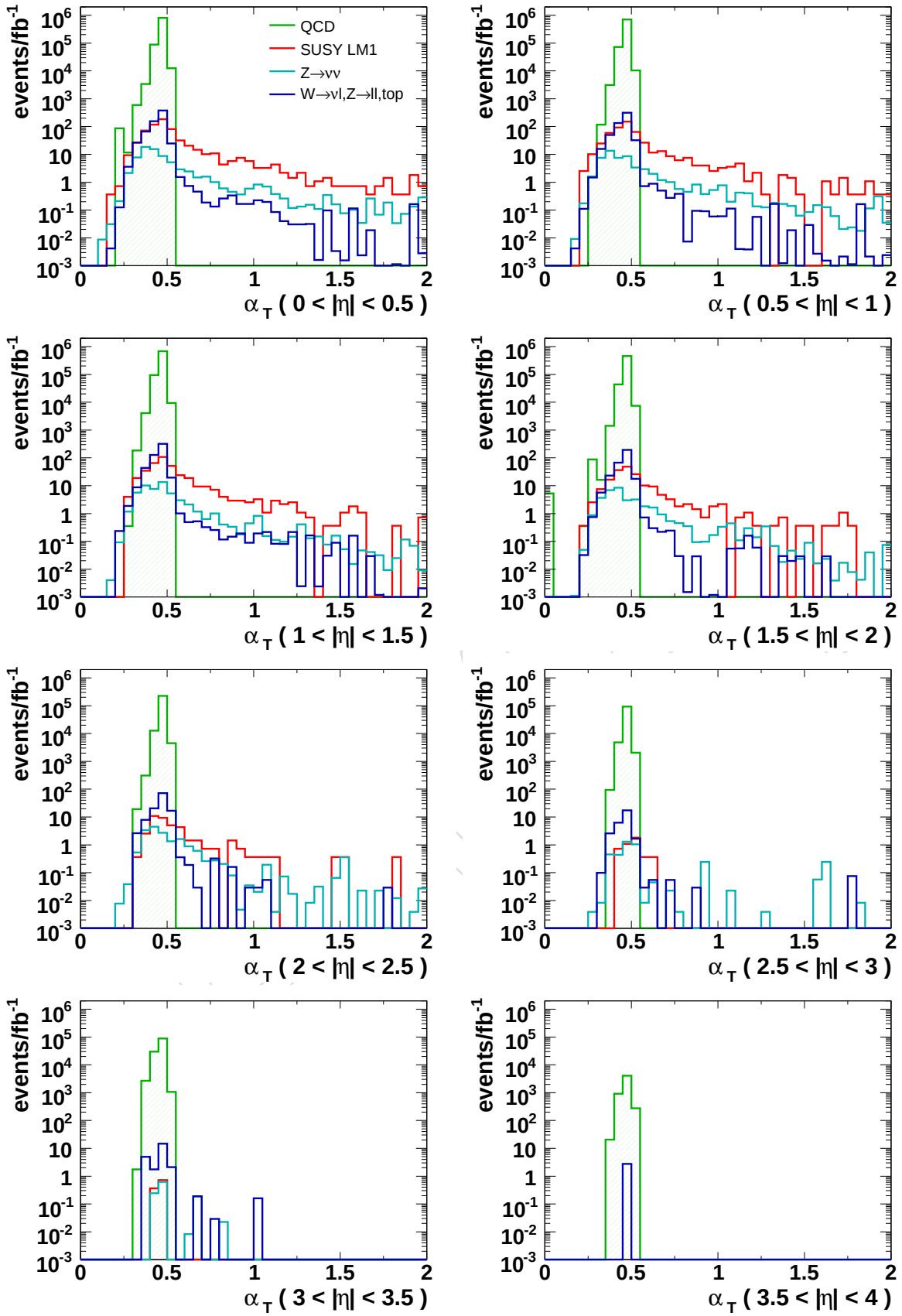

Figure 10: Distribution of α_T for QCD, $t\bar{t}$, W, Z, and SUSY events in different bins of $|\eta|$ of the leading jet. Shown is the expected number of events for a luminosity of 1fb^{-1}, after all selection cuts except the cut on α_T and $|\eta|$ of the leading jets

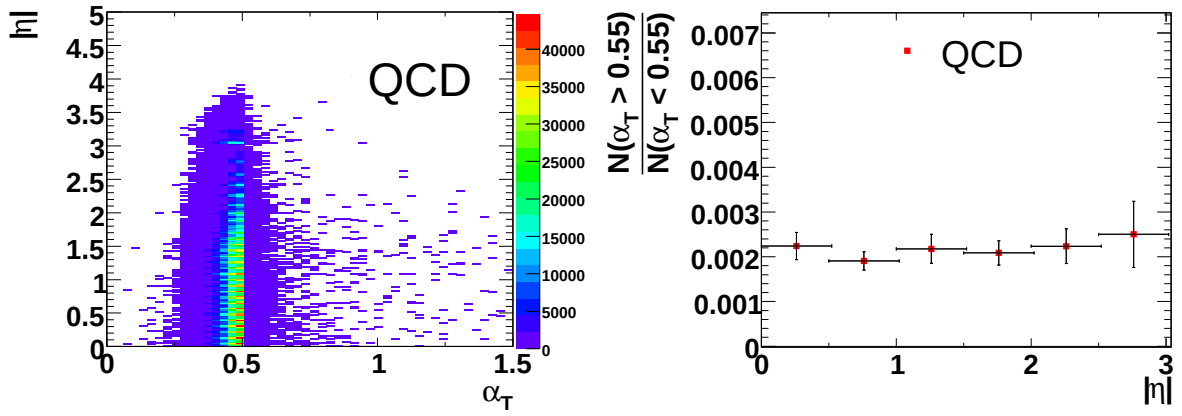

Figure 11: Left: α_T versus $|\eta|$ of the leading jet for QCD dijet events. Right: R_{α_T} as a function of $|\eta|$ after all selection cuts except those on α_T and $|\eta|$. The cut on $p_T^{j3}$is loosened to 200 GeV.

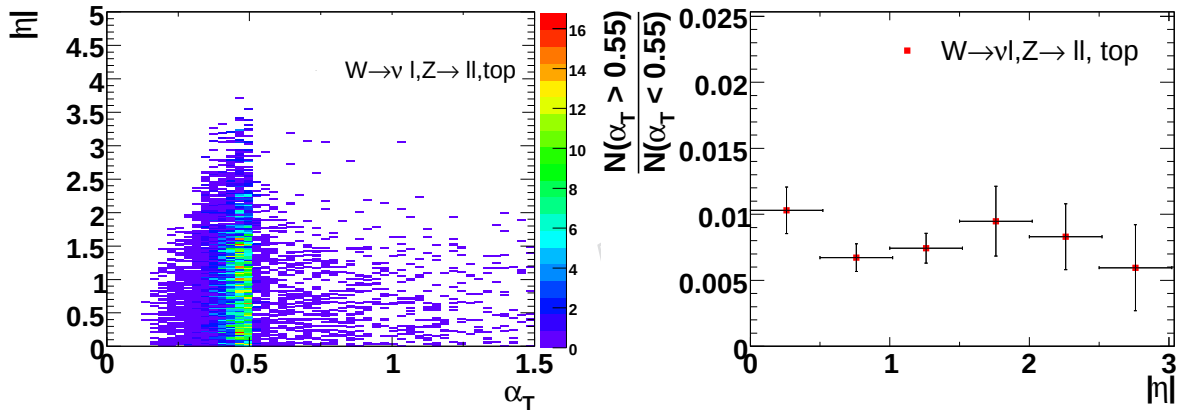

Figure 12: Left: α_T, versus $|\eta|$ of the first jet for $t\bar{t}$, $W \to \ell\nu$ and $Z \to \ell\ell$ events. Right: R_{α_T} as a function of $|\eta|$ for $t\bar{t}$, $W \to \ell\nu$ and $Z \to \ell\ell$ events. Shown after the application of all selection cuts except the cut on α_T and $|\eta|$.

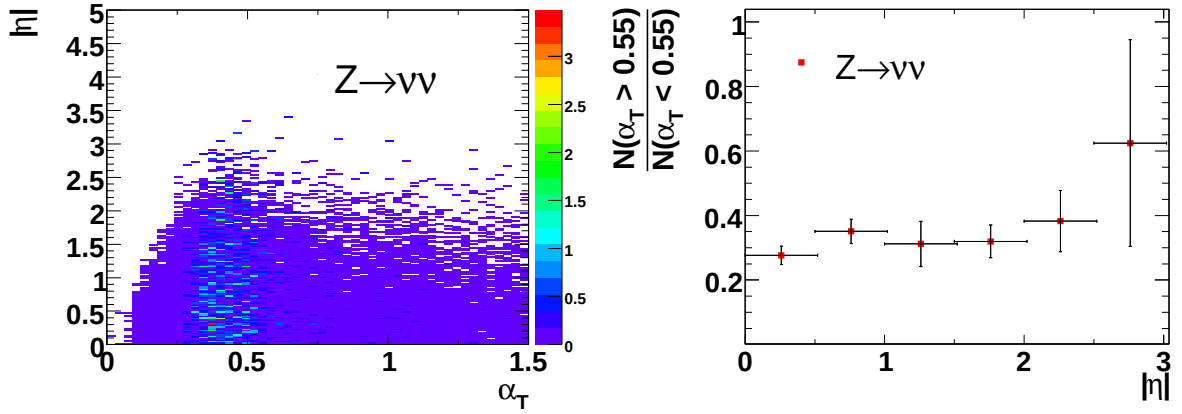

Figure 13: Left: α_T versus $|\eta|$ of the first jet for $Z \to \nu\nu$ events. Right: R_{α_T} as a function of $|\eta|$ for $Z \to \nu\nu$ events after application of all selection cuts except the cut on α_T and $|\eta|$.

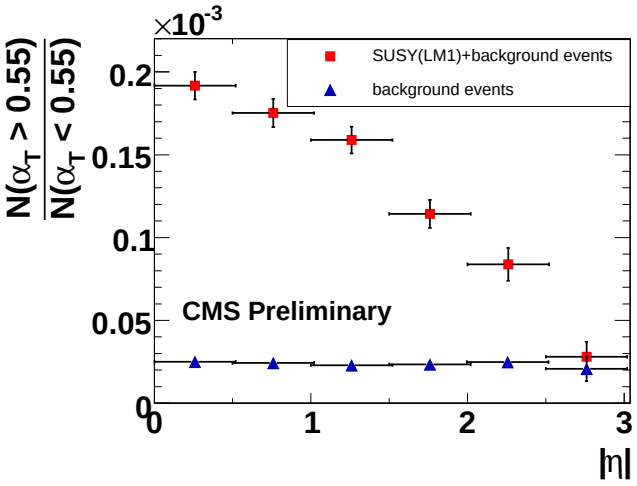

Figure 14: R_{α_T} as a function of $|\eta|$ of the leading jet after all selection cuts except the cut on α_T and $|\eta|$. Shown once for background events only (blue triangles) and for a mixture of background and SUSY events for LM1 (red squares).

distributed in α_T and $|\eta|$ of the leading jet. In Figure 13 R_{α_T} is shown as a function of $|\eta|$ after all selection cuts except the cut on α_T and $|\eta|$. The large fluctuation for high $|\eta|$ values is due to the difference between the number of simulated events and the number of expected events for an integrated luminosity of $1 fb^{-1}$.

7.1.2 Results of the combined background estimation using the matrix method

As we have seen in the previous section, R_{α_T} is to good approximation constant for all the relevant background contributions, it is therefore legitimate to combine all the backgrounds and determine them "in one go". R_{α_T} is shown for all backgrounds combined in Figure 14. As can be seen also the combined R_{α_T} is flat as a function of $|\eta|$. The value of R_{α_T} determined in the forward region $|\eta| > 2.5$ is $R_{\alpha_T} = (2.1 \pm 0.7) \cdot 10^{-5}$.

To estimate the number of background events in the $|\eta| < 2.5$ regions, $N_{\text{pred}}(|\eta|)$, R_{α_T} needs to be multiplied with the number of of event with $\alpha_T < 0.55$, $N_{\text{bkgd}}(|\eta|)$ in the corresponding $|\eta|$ bin.

$$N_{\text{pred}}(|\eta|) = R_{\alpha_T} \cdot N_{\text{bkgd}}(|\eta|) \tag{5}$$

Figure 15 shows the number of predicted and the number of measured background events after all selection cuts in the different $|\eta|$ regions. The two agree very well within errors. In addition, in Figure 15 the the number of signal plus background events is compared to the number of predicted events. The signal is clearly visible above the background.

In table 6 the absolute number of predicted and simulated background events with $|\eta| < 2.5$ and $\alpha_T > 0.55$ are given. The prediction is done once in the case that SUSY is realized in nature at parameter-point LM1 and once for the case that SUSY is not realized in nature. The method predicts correctly (within the statistical uncertainty) the background in the central region. The presents of SUSY (LM1) would lead to an overestimation of the background of about 20%, but still the measured events in the signal region would be far above (factor 5.6) the predicted background.

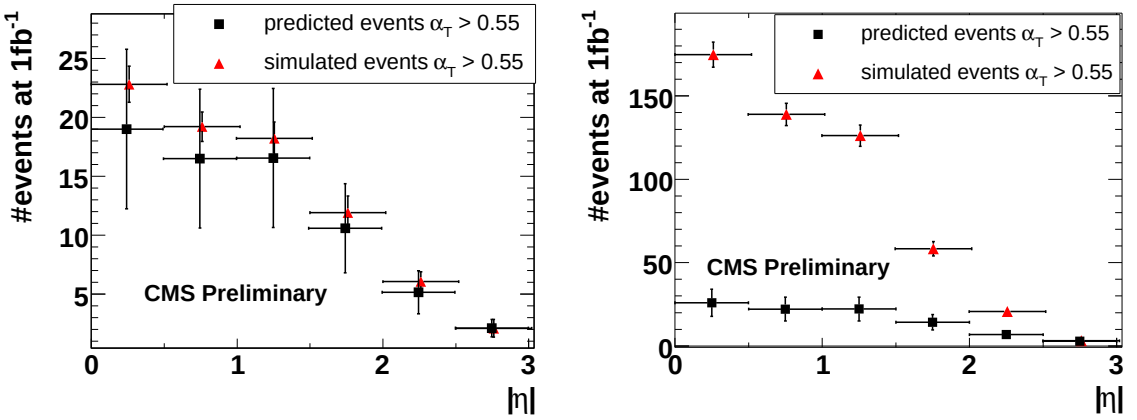

Figure 15: Comparison of the number of predicted events and the simulated number of events for a luminosity of 1 fb^{-1} with $\alpha_T > 0.55$. a) Shown for the case that SUSY is not realized in nature and only background events can be measured. The predicted number of events are shown in black while the simulated number of events is shown in red. Both agree within errors. b) Shown for the case that SUSY is realized at the parameter-point LM1. Red is the number of simulated background plus SUSY events. Black is the number of predicted background events. The signal is well visible above the background.

Table 6: Number of simulated events in the signal region ($\alpha_T > 0.55$ and $|\eta| < 2.5$) compared to the number of predicted background events using the Matrix Method. The prediction is done once in the case that SUSY is not realized in nature (and does not affect the background prediction), and once for the case that SUSY is realized at parameter-point LM1 (and thus influences the prediction). The errors refer to statistical errors due to the finite size of the samples of simulated events. In parentheses are the statistical uncertainties expected for a data sample of 1fb^{-1}.

Predicted background	Simulated background	Predicted background (with SUSY LM1)	Simulated background and SUSY LM1
68 ± 24 (± 43)	77 ± 3 (± 8)	91 ± 30 (± 51)	517±13 (±22)

7.1.3 Stability of matrix method

The stability of the presented matrix method was verified against the systematic variations discussed in Sec. 6.1. In each case the predicted number of background events is compared with the number of events present in the MC sample (simulated), assuming either no signal contamination or the presence of a LM1 signal. As through the systematic variations only a few events get moved across the $\alpha_T = 0.55$ border (in the region $|\eta| > 2.5$) the results are strongly correlated. The results are given in Table 7.

7.1.4 Validity test of the Matrix Method with real data

The validity of this method can be estimated directly from data. For this the selection cuts are loosened until the signal contribution becomes negligible. Then the measured ratio between the number of events with $(\alpha_T > 0.55)$ and the number of events with $(\alpha_T < 0.55)$ should be flat in $|\eta|$.

Figure 16 shows the ratio for a mix of SUSY LM1 and background events for several different HT cuts. If the HT cut is loosened below 300 GeV the ratio remains approximately flat. Figure

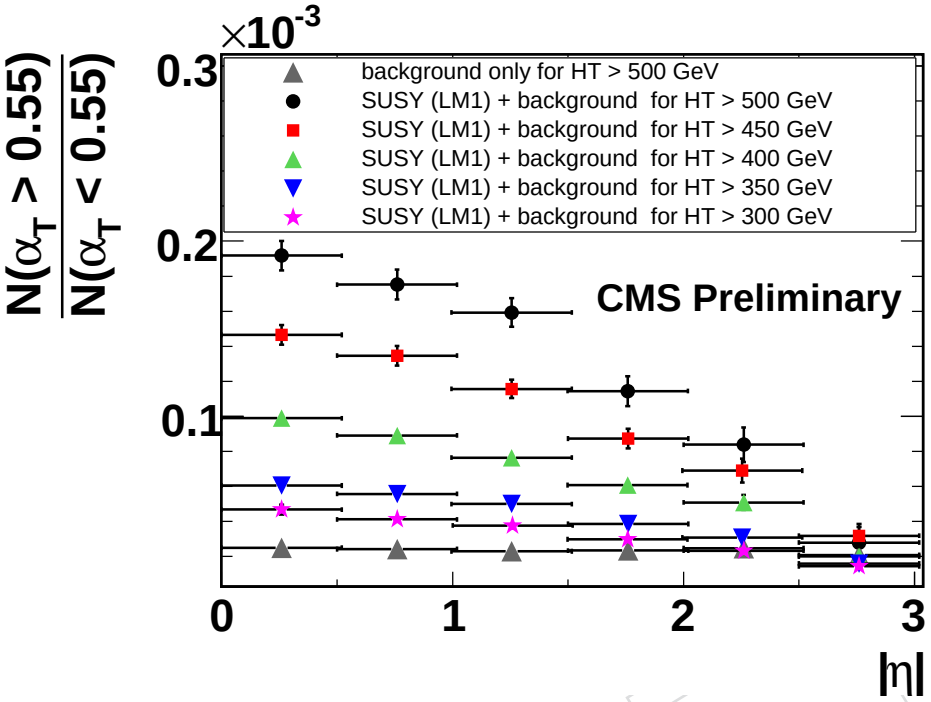

Figure 16: Ratio of the number of events with $\alpha_T > 0.55$ and the number of events with $\alpha_T < 0.55$ as a function of $|\eta|$ for different HT cuts.

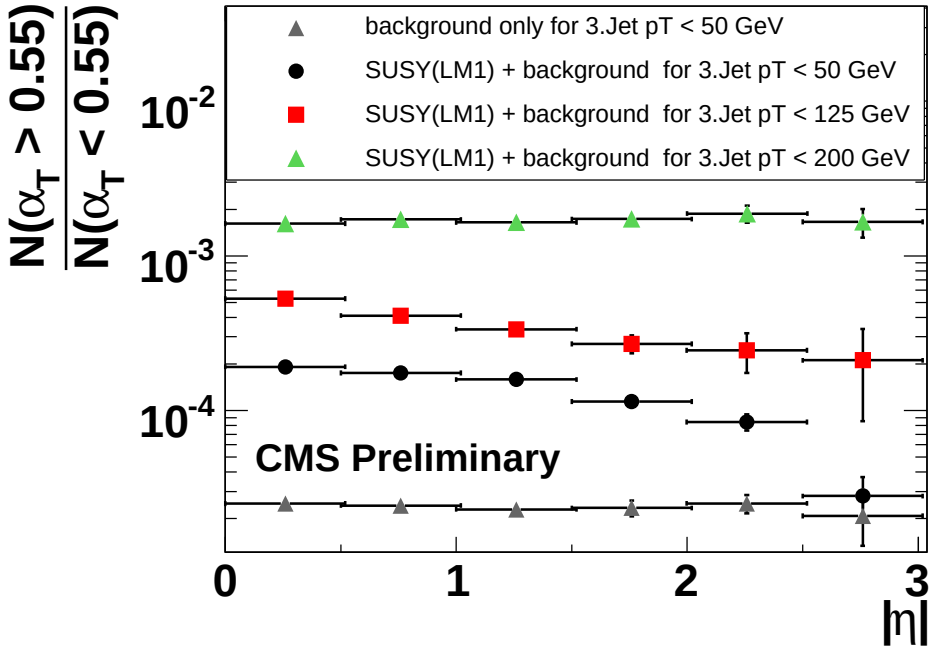

Figure 17: Ratio of the number of events with $\alpha_T > 0.55$ and the number of events with $\alpha_T < 0.55$ as a function of $|\eta|$ for different cuts on the p_T of the third leading jet.

Table 7: Number of simulated and predicted background events in the signal region ($\alpha_T > 0.55$ and $|\eta| < 2.5$) for the various systematic variations. The quoted uncertainties correspond to the available MC statistics.

Systematic variation	Predicted background	Simulated background	Predicted background (with SUSY LM1)	Simulated background and SUSY LM1
10% E_{T} smearing and 0.1 rad $\Delta\phi$ smearing	65 ± 23	75 ± 3	88 ± 29	501 ± 13
Jet energy scaling by +5%	62 ± 22	94 ± 4	123 ± 33	555 ± 13
Jet energy scaling by −5%	46 ± 23	68 ± 3	71 ± 24	456 ± 12
Jet energy scaling by +3% ($\|\eta\| > 1.4$)	48 ± 17	81 ± 3	65 ± 21	521 ± 13
Jet energy scaling by −3% ($\|\eta\| > 1.4$)	73 ± 31	78 ± 3	91 ± 29	517 ± 13

17 shows the same plot but with loosened cuts on the third leading jet p_T. Here the ratio changes with the cut on the third jet pt as more genuine three jets are selected for which α_{T} can have values greater than 0.55. In addition to that the signal contribution becomes negligible. This is one of the checks to be done once data is available.

7.2 Estimating the Z $\longrightarrow \nu\bar{\nu}$ background with the help of W + jets events

To estimate the jets + Z to invisible background the W + jets channel can be utilized as cross check to the forward extrapolation method discussed in the previous section. Given the larger cross-section, Ws will be reconstructed with greater statistics than Zs. Once a clean W sample is selected it still needs to be normalized to the Zs, which can be done either from data or with the help of Monte Carlo simulations. Except for the W identification via an isolated muon, the selection is kept exactly the same as for the final analysis. Similar strategies have been studied in detail for the $\geq$3 jet SUSY searches [13].

7.2.1 W $\longrightarrow \mu\nu$ and Z $\longrightarrow \mu\mu$ selection

We start by selecting an isolated global muon. The muon isolation is done only track-based, since QCD background after the selection cuts is largely suppressed. The transverse momentum of tracks within a cone of ΔR of 0.3 is required to be less than 9% of the transverse momentum of the muon. This isolation is also proposed for the W cross section measurement [14] and similarly in the Z to invisible background estimation for SUSY searches with larger jet multiplicities [13]. The transverse momentum of the muon needs to be greater than 25 GeV. For the selection of W in the signal region $\alpha_{\mathrm{T}} > 0.55$ all cuts of the final analysis are applied. Only the muon veto is ignored if exactly one muon with the above criteria is found. This leads to a clean W sample with 48.7 events selected with an purity of 92%. The only significant backgrounds are $t\bar{t}$(3.2 events) and a small amount of Z plus jets (0.9 events). If desired the $t\bar{t}$background to the W selection could be reduced by b-tagging and in addition it can also be estimated by data-driven methods [13].

For the search presented here the largest W contamination might be due to the SUSY signal. For the given selection 18.8 events from SUSY at LM1 would remain. However, W events passing

the final selection need to have Ws with a momentum of several 100 GeV as shown in Figure 18. The transverse mass of the two jets can only be significantly reduced if a large fraction of the transverse momenta is carried away. Hence the α_t cut is strongly correlated to the W transverse momentum. The selection leads to a boost of the isolated muons and hence large transverse momentum (Figure 19). The correlation between the muon and the W can be used to define further selection criteria to reduce background, namely the $\Delta\phi$ between the muon and MHT (Figure 20) and the ratio between the transverse momentum of the muon and MHT. The final selection of W is summarized in Table 8. 37.5 W candidates are selected, of which 1.8 are $t\bar{t}$and 0.7 Z plus jets. No LM1 SUSY contamination remains after this selection.

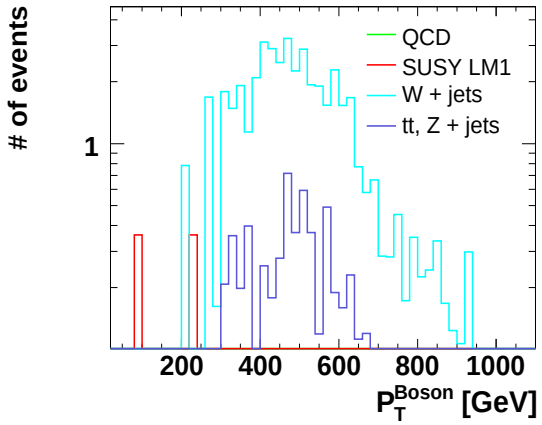

Figure 18: True transverse momentum of Bosons after standard selection.

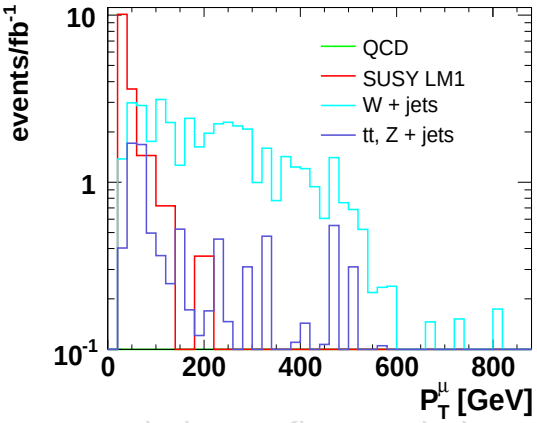

Figure 19: Reconstructed transverse momentum of the muon after standard selection.

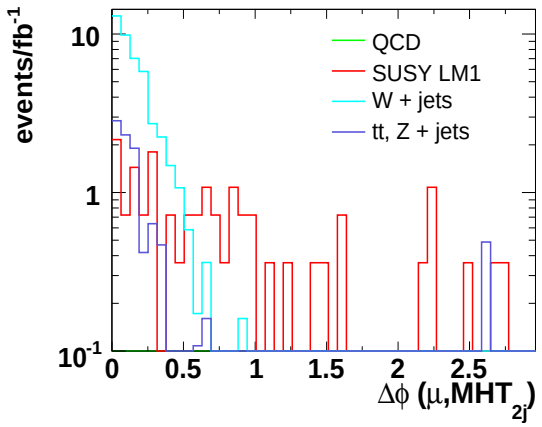

Figure 20: $\Delta\phi$ between MHT$_{2j}$ and the muon.

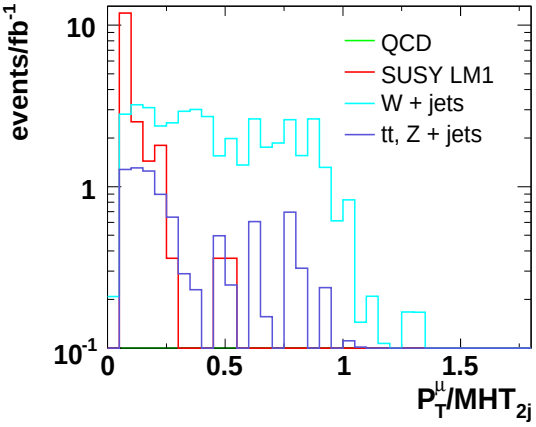

Figure 21: Ratio of transverse momentum and MHT$_{2j}$.

The selection of Z in the signal region is straight forward since no background remains. A pair of global muons with an invariant mass difference to the nominal Z mass of less than 10 GeV is selected as Z candidates. The selection in 100% pure and 3.6 events are expexted after all

Table 8: Selection criteria for W and Z in the signal region.

W	1 global muon	track iso	$P_t^\mu > 25\,\text{GeV}$	$P_t^\mu / MHT > 0.25$	$\Delta\phi(\mu, MHT) < 0.75$
Z	2 global muons	opposite ch.	$P_t^\mu > 15\,\text{GeV}$	$\lvert M_{\mu^-\mu^+} - M_Z \rvert < 10\,\text{GeV}$	

Table 9: W and Z after final cuts in from Monte Carlo truth and reconstruction.

	W_{cand}	W_{true}/W_{cand}	Z_{cand}	Z_{true}/W_{true}	$Z \to \nu\bar{\nu}$
HT $>$ 300 GeV	186.6	1.43	20.1	0.20	366.2 ± 27
HT $>$ 500	37.5	1.44	3.6	0.19	61.6 ± 10.1

selection criteria of the analysis are applied, except for the muon veto, which is ignored if a Z candidate is found. If contamination of SUSY is of concern, then the correlation between MHT and the muons could also be exploited for the Z selection.

7.3 Normalization of $W \to \mu\nu$ to $Z \to \nu\bar{\nu}$

The number of true W can be extracted from data provided the acceptance (ϵ_a) is known from Monte Carlo simulations and the muon isolation and reconstruction efficiency (ϵ_{reco}) can be determined. An procedure for determination of the muon isolation efficiency as a function of η from the data is described in [14] where an efficiency above 95% is achieved. In our study $\epsilon_a \times \epsilon_{reco}$ is taken from Monte Carlo simulations as the ratio of reconstructed over true W events. Where true W are events that passed all cuts except the muon veto and are known to be W from Monte Carlo truth. For the Z the true number of events after all cuts but the muon veto could be used as well. To avoid differences from the different generator used for $Z \to \nu\nu$ (PYTHIA) and $Z \to \mu\mu$ (ALPGEN) the true number of events for the Z is taken from the $Z \to \nu\nu$ events passing all cuts divided by 6. This difference of the generators will not occur in nature and hence this not included in this closure test of the method. In the future it will be possible to take the ratio of true W and true Z in the two jet channel from tuned Monte Carlo simulations. Studies to determine these at LHC are planned within the CMS electroweak physics analysis group. In this study this ratio is taken from Monte Carlo truth. The resulting numbers are shown in Table 9. The number of true $Z \to \nu\bar{\nu}$ events can be estimated as:

$$Z \to \nu\bar{\nu}_{\text{estimated}} = \mathbf{W_{cand}} \times \mathbf{W_{true}/W_{cand}} \times \mathbf{Z_{true}/W_{true}} \times \mathbf{6} = \mathbf{61.6 \pm 10.1}$$

The factor 6 in Eq. 7.3 stems from the V-A relation for the ratio of $Z \to \nu\bar{\nu}$ to $Z \to \mu\mu$. The quoted uncertainty is statistical only. However, the ratio of W/Z from Monte Carlo might have large uncertainties and could be determined also from data. To increase the statistics of the reconstructed W and Z the HT cut is relaxed to $HT > 300\,\text{GeV}$. This leads to 187 W candidates, of which 18 are $t\bar{t}$and 3 Z+jets events, and 20 Z candidates with 100% purity. The events selected this way are close enough in phase space to assume a constant ratio of Z and W for the two HT requirements. Only 0.7 events of the LM1 SUSY sample passed the relaxed cuts. Clearly dominating is the statistical uncertainty due to the small number of reconstructed Z. This method would lead to an estimation of 65.4$\pm$ 16.9 Z to invisible. Compared to the quoted uncertainty, the uncertainty from acceptance and efficiency is negligible.
The expected numbers of $Z \to \nu\bar{\nu}$ background of this closure test agree well background of the 58.2 events expected in the presented SUSY search.

The very specific correlation between MHT and the leptons of the decaying W and Z bosons

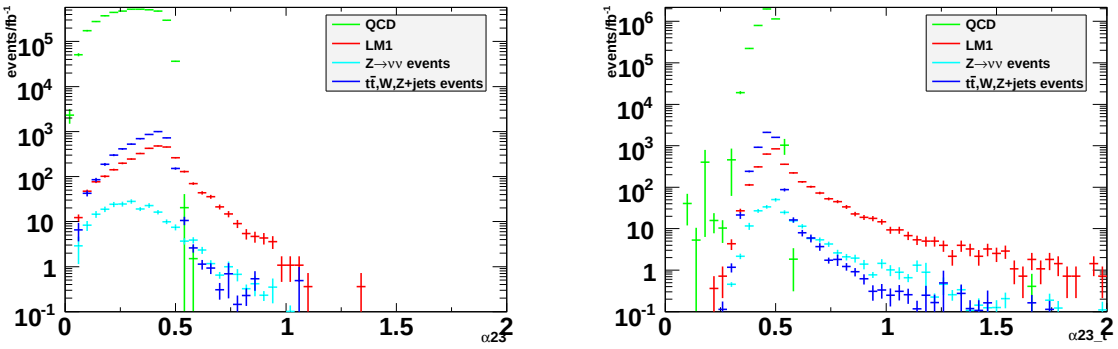

Figure 22: Distribution of α^{3jet} and $\alpha_{\mathrm{T}}^{3jet}$, after all other selection cuts have been applied.

could also be used to extend this strategy to W and Z's decaying to electrons to increase statistics and crosscheck results. An alternative strategy would be to use γ + jets events to estimate the Z to invisible background. This is exercised in [13] for multiple jet searches in SUSY and could also be adopted to this analysis.

8 Extension of the method to three jet events

The dijet analysis presented in this note can easily be extended to three jets. This might be of interest in case the rate of extra hard jets from higher order QCD processes is larger than predicted from the currently available simulation tools and so some of the signal events that we currently classify as dijet events would show up as events with three jets. Nevertheless the QCD background can still be controlled as transverse momentum conservation still applies. We proceed by absorbing a third jet in the definition of α (α_{T}) in a procedure similar to Bremsstrahlung recovery for electron-photon pairs. For this we add the four-vectors of the second and third hardest jet in the event to form a combined jet and then calculate α (α_{T}) as before from the leading jet and the newly formed combined jet.

In the three jet case the dijet selection needs to be adapted slightly. Instead of vetoing a third jet we now select such a jet with $p_T^{j3} > 50\,\mathrm{GeV}$ and require a possible fourth jet to have $p_{\mathrm{T}}^{j4} < 50\,\mathrm{GeV}$. Similarly we adapt the HT definition and due to limited experimental resolution we slightly tighten the cut on α_{T}, resulting in:

- $p_T^{j3} > 50\,\mathrm{GeV}$
- $p_{\mathrm{T}}^{j4} < 50\,\mathrm{GeV}$
- $\mathrm{HT} = p_T^{j1} + p_T^{j2} + p_T^{j3} > 500\,\mathrm{GeV}$
- $\alpha_{\mathrm{T}} > 0.57$

With this definition we obtain a data sample complementary to the dijet sample. In Figure 22 we show the resulting $\alpha_{\mathrm{T}}^{3jet}$ distribution. As before a sharp edge at $\alpha_{\mathrm{T}} = 0.5$ is visible despite the slightly worsened α_{T} resolution.

With the selection described above in place we show the event yields for the background processes and the benchmark LM1 point in Table 10. The significantly larger signal yield can be attributed to $\tilde{\mathrm{q}}\,\tilde{\mathrm{g}}$ production contributing much stronger when requiring three jets with $p_{\mathrm{T}} > 50\,\mathrm{GeV}$.

Table 10: Event yields for 3 jet events using α_T^{3j}.

Selection	QCD	$t\bar{t}$,W,Z+jets	$Z \rightarrow \nu\bar{\nu}$	LM1	S/B
α	0	6.6	9.9	195	11.8
α_T	1.9	39	56	761	7.9

The same data-driven background estimation techniques as discussed in Sec. 7 should also be applicable to the three jet analysis.

9 Conclusions

We have carried out a search for a low mass SUSY signature using dijet events. This represents an extension to the existing SUSY searches at CMS which so far have been based on ≥ 3 jets + missing E_T. In our study we have explored two new kinematic variables, α and α_T, which are very powerful in suppressing the several orders of magnitude larger background from QCD dijet events. Exploiting the discrimination power of α (α_T) we have shown that several SUSY benchmark points can be discovered with a data sample of 1 fb^{-1} where signal over background ratios of up to 6 were achieved. Furthermore we developed two independent data-driven techniques for background estimation. By defining signal depleted and enriched regions in the leading jet η we showed that a modified matrix method can be used to predict the total number of background events in the barrel with $\alpha_T > 0.55$. In an alternative approach that can be used as a cross-check we showed how to use W+jets event to determine the dominant $Z \rightarrow \nu\bar{\nu}$ background. Finally, our results show that for a favourable signal like the LM1 benchmark point a discovery would be possible with as little as 100 pb^{-1}.

References

[1] L. Randall and D. Tucker-Smith, "Dijet Searches for Supersymmetry at the LHC," arXiv:0806.1049.

[2] **CMS** Collaboration, G. L. Bayatian et al., "CMS technical design report, volume II: Physics performance," *J. Phys.* **G34** (2007) 995–1579. doi:10.1088/0954-3899/34/6/S01.

[3] https://twiki.cern.ch/twiki/bin/view/CMS/SusyPat.

[4] https://twiki.cern.ch/twiki/bin/view/CMS/SWGuidePAT.

[5] https://twiki.cern.ch/twiki/bin/view/CMS/SusyPatCrossCleaner.

[6] https://twiki.cern.ch/twiki/bin/view/CMS/CSA07Physics.

[7] T. Sjostrand et al., "High-energy-physics event generation with PYTHIA 6.1," *Comput. Phys. Commun.* **135** (2001) 238–259, arXiv:hep-ph/0010017. doi:10.1016/S0010-4655(00)00236-8.

[8] M. L. Mangano, M. Moretti, F. Piccinini, R. Pittau, and A. D. Polosa, "ALPGEN, a generator for hard multiparton processes in hadronic collisions," *JHEP* **07** (2003) 001, arXiv:hep-ph/0206293.

[9] https://twiki.cern.ch/twiki/bin/view/CMS/GeneratorProduction2007CSA07Signal.

[10] W. Beenakker, R. Hopker, M. Spira, and P. M. Zerwas, "Squark and gluino production at hadron colliders," *Nucl. Phys.* **B492** (1997) 51–103, arXiv:hep-ph/9610490. doi:10.1016/S0550-3213(97)00084-9.

[11] **D0** Collaboration, V. M. Abazov et al., "Measurement of dijet azimuthal decorrelations at central rapidities in $p\bar{p}$ collisions at $\sqrt{s} = 1.96$ TeV," *Phys. Rev. Lett.* **94** (2005) 221801, arXiv:hep-ex/0409040. doi:10.1103/PhysRevLett.94.221801.

[12] https://hypernews.cern.ch/HyperNews/CMS/get/simDevelopment/1043/4/2/1.html.

[13] CMS Physics Analysis Summary, CMS PAS SUS-08-002.

[14] CMS Physics Analysis Summary, CMS PAS EWK-07-002.